# AQP9 transports lactate in tumor-associated macrophages to stimulate an M2-like polarization that promotes colon cancer progression

Yundi Shi [a], Masato Yasui [a,b], Mariko Hara-Chikuma [a,*]

[a] *Department of Pharmacology, Keio University School of Medicine, Japan*
[b] *Center for Water Biology and Medicine, Keio University Global Research Institute, Japan*

A B S T R A C T

Macrophages play a major role in the immune defense against pathogenic factors; however, they can lead to tumor exacerbation and metastasis, as the tumor microenvironment (TME) polarizes tumor-associated macrophages (TAMs) into the M2 subtype. Lactate, a metabolite produced by carcinoma cells at high concentrations in the TME, induces an M2-polarization in macrophages, which ultimately leads to the secretion of factors, such as vascular endothelial growth factor (VEGF), and promotes tumor progression. However, the effect of TAM lactate import on tumor progression has not been fully elucidated. Aquaporin 9 (AQP9) is a transporter of water and glycerol expressed in macrophages. Here, we used a tumor allograft mouse model to show that AQP9 knockout (AQP9$^{-/-}$) mice were more resistant against tumor cell growth and exhibited a suppressive M2-like polarization in tumor tissue than wild-type mice. Moreover, we discovered that the primary bone marrow-derived macrophages from AQP9$^{-/-}$ mice were less sensitive to lactate stimulation and exhibited reduced M2-like polarization as well as decreased VEGF production. To further investigate the role of AQP9 in macrophage polarization, we overexpressed AQP9 in Chinese hamster ovary cells and found that AQP9 functioned in lactate import. In contrast, primary AQP9$^{-/-}$ macrophages and AQP9 knockdown RAW264.7 cells exhibited a reduced lactate transport rate, suggesting the involvement of AQP9 in lactate transport in macrophages. Together, our results reveal the mechanism by which the TME modifies the polarization and function of tumor-infiltrating macrophages via AQP9 transport function.

## 1. Introduction

Cancer results in around 10 million deaths every year and became the second worldwide leading cause of death after heart disease in 2020 [1]. Colon cancer is an adenocarcinoma that develops from the colon or rectum and is the third most diagnosed type of cancer in men [2]. With in-depth research investigating the molecular mechanism of colon cancer adenocarcinoma (COAD), the molecular treatment options have increased rapidly in recent years [3]. However, despite progress associated with the development of chemotherapy and molecularly targeted therapies, the survival time and rate of patients with colon cancer remain low. Therefore, it is important to identify the key factors that influence survival in colon cancer [4].

The tumor microenvironment (TME) is known to be related to cancer progression in solid cancers, including colon cancer [5]. The TME is a complex ecosystem in which cancer cells crosstalk with immune cells, such as T cells, monocytes, and tumor-associated macrophages (TAMs)

[6]. Monocytes are innate immune cells that are recruited into the TME and are essential for tumor progression due to their capacity to secrete immune cytokines or differentiate into macrophages to participate in cancer metastasis and progression [7–9]. TAMs derived from monocytes play an important role in tumor progression, which is associated with poor outcomes in patients with colon cancer [10,11]. Within the TME, TAMs are categorized into two subtypes, M1 and M2. M1 polarization is associated with inflammation and anti-tumor responses by directly lysing cells after phagocytosis and indirectly enhancing the function of other immune cells [12,13]. In contrast, M2-like TAMs are associated with remodeling and tumor promotion by secreting immunosuppressive cytokines and inducing angiogenesis via VEGF expression [14].

The lactate produced by cancer cells represents one of the main factors that promote pro-tumoral M2-like TAMs in the TME [15]. Elevated lactate induces M2 macrophage polarization through the activation of the ERK/STAT3 signaling pathway and Gpr132, which aggravates tumor progression and promotes angiogenesis [16–18]. Lactate can also inhibit ATP6V0d2 expression in TAMs and increase

**Abbreviations**

| | |
|---|---|
| AQP9 | aquaporin-9 |
| AQP9$^{-/-}$ | Aquaporin-9 knockout |
| AQP9-CHO | AQP9 overexpressing Chinese hamster ovary cell |
| MCT1-CHO | MCT1 overexpressing Chinese hamster ovary cell |
| ARG1 | arginase 1 |
| BCECF | 2',7'-Bis-(2-carboxyethyl)-5-(and-6)-carboxyfluorescein |
| BMDMs | bone marrow-derived macrophages |
| CCL2 | chemokine (C–C motif) ligand 2 |
| CCR2 | chemokine (C–C motif) receptor 2 |
| CHO cell | Chinese hamster ovary cell |
| COAD | colon cancer adenocarcinoma |
| CXCL12 | chemokine (C-X-C motif) ligand 12 |
| CXCR4 | chemokine (C-X-C motif) receptor 4 |
| FACS | fluorescence-activated cell sorter |
| IFN-γ | interferon gamma |
| iNOS | nitric oxide synthase 2 |
| LPS | lipopolysaccharide |
| Ly6C | lymphocyte antigen 6 complex, locus C1 |
| Ly6G | lymphocyte antigen 6 complex, locus G |
| MFI | mean fluorescence intensity |
| MCT1 | monocarboxylate transporter 1 |
| RCC | renal cell carcinoma |
| TCM | tumor-conditioned medium |
| TAM | tumor-associated macrophages |
| TGF-β | transforming growth factor, beta |
| VEGF | vascular endothelial growth factor A |

VEGF expression via HIF-2α [19]. However, the effect of TAM lactate import on tumor progression has not been fully elucidated. We hypothesized that the inhibition of lactate uptake could have anti-tumor effects by affecting macrophage polarization.

Aquaporins (AQPs) are a family of channel-forming proteins that are expressed broadly in all types of tissues and facilitate the movement of water through the membrane using osmotic and solute gradients [20]. Aquaporin-9 (AQP9), a member of the aquaporin family, transports water and small molecules, including glycerol and hydrogen peroxide [21,22]. AQP9 was found to be expressed in cancer cells and various immune cells, such as neutrophils, T cells, and macrophages [23–26]. Previous studies have shown that AQP9 expression in cancer cells is associated with worse relapse-free survival in renal cell carcinoma (RCC) and breast cancer [27,28]. *In vitro* studies have suggested that AQP9 knockdown in RCC cells inhibits the malignant phenotypes of cells via the pre-miR-532 signaling pathways [29]. Conversely, our preliminary analysis using the Gene Set Cancer Analysis database [30] showed that AQP9 expression levels in tumor tissues of patients with COAD were correlated with cancer stage and prognosis (Supplementary Figs. S1A–C). In particular, AQP9 was found to be highly expressed in infiltrated macrophages (Supplementary Figs. S1D and E). However, the role of AQP9 expression in TAMs has not yet been elucidated.

Here, we investigated whether macrophages expressing AQP9 in the TME are involved in cancer progression via its transporter function. Using AQP9 knockout (AQP9$^{-/-}$) mice and a tumor allograft model, we showed that AQP9$^{-/-}$ mice resisted tumor growth via reduced transition into M2-like macrophages caused by the blockage of lactate transport.

## 2. Materials and methods

### 2.1. Mice

C57BL/6 wild-type (WT) mice were obtained from SLC Inc. (Japan). AQP9$^{-/-}$ mice (C57BL/6 genetic background) were provided by Dr. Aleksandra Rojek and Soren Nielsen at Aarhus University [26,31]. The AQP9 knockout status was verified by western blotting and qPCR (Supplementary Figs. S1F and S1G). All animal experiments were carried out using 8–10 weeks old male littermates and approved by the President of Keio University, following the approval of the Institutional Animal Care and Use Committee of Keio University (approval no. 16075) and by the Genetic Modification Safety Committee, Keio University School of Medicine (approval no. 28–029). All experiments were performed according to institutional procedures, national guidelines, and relevant national laws on the protection of animals.

### 2.2. Syngeneic tumor model

MC38 cells ($2 \times 10^5$ cells in 100 μl) were injected subcutaneously

into the right abdominal flank of WT and AQP9$^{-/-}$ mice. Two weeks following tumor inoculation, tumor diameters were measured with a digital caliper every 2 days after becoming palpable. Tumor volume was calculated using the formula (width × width × length)/2 [32]. Mice were euthanized, and the tumor tissues were harvested and weighed.

### 2.3. Bone marrow-derived macrophage (BMDM) preparation and culture

BMDMs were prepared as previously described [33]. Briefly, single-cell suspensions of bone marrow cells were collected from the femur and tibia and resuspended in RPMI 1640 (Invitrogen) supplemented with 10% fetal bovine serum (FBS), 100 U/ml penicillin and 100 μg/ml streptomycin. Cells were plated onto dishes and incubated with 10 ng/ml GM-CSF (R&D) and 50 μM 2-mercaptoethanol for at least 6 days. FACS analysis was performed to assess the purity of macrophages, and >90% of the cultured cells were confirmed as macrophages. For further macrophage polarization study, cells were incubated with 1 ng/ml lipopolysaccharide (LPS) and 10 ng/ml IFN-γ to obtain M1 macrophages, and with 20 ng/ml IL-4 or 25 mM lactate acid to obtain M2 macrophages.

### 2.4. Cell culture and transfection

Chinese hamster ovary cells (CHO–K1 cells, Riken BRC cell bank, Japan), RAW 264.7 cells (mouse macrophages, Riken BRC cell bank, Japan), and MC38 cells (murine colon adenocarcinoma cells, provided by Dr. James P. Allison, Memorial Sloan Kettering Cancer Center, New York, USA), were maintained in Dulbecco's modified Eagle's medium (DMEM) supplemented with 10% FBS, 100 U/ml penicillin and 100 μg/ml streptomycin. The cDNA plasmid for AQP9 mice (pCMV6 vector, Origene) was transfected into CHO cells using the Lipofectamine 3000 reagent (Invitrogen). Subsequently, the cells were selected using G418 treatment. For RNA interference knockdown, subconfluent RAW 264.7 cells were transfected with 5 nM AQP9- or non-targeting-siRNA (ON-TARGET plus SMARTpool, Thermo Fisher Scientific) with Lipofectamine 3000 (Invitrogen) according to the manufacturer's protocol. After 48 h of transfection, cells were harvested for further analysis.

### 2.5. FACS analysis

To obtain single-cell suspensions, tumor tissue was fragmented in PBS and incubated for 60 min at 37 °C with 25 μg/ml of the liberase enzyme (Roche) and pipetted every 20 min. After incubation, the suspensions were filtered using a 70 μm strainer and centrifuged for 5 min at 1000 rpm to collect the cell pellets. Cells were then stained with antibodies before analysis using a FACS CytoFLEX S flow cytometer (Beckman). Data were analyzed using the FlowJo software.

## 2.6. Chemotaxis assay

Chemotaxis assays were performed as described previously [26]. Bone marrow-cells from WT and AQP9$^{-/-}$ mice were collected and deposited in the upper chamber containing a polycarbonate transwell membrane filter (5-μm pore size; Corning) for 2 h. The lower chamber contained 20 ng/ml CCL2 or 100 ng/ml CXCL12 in 0.5% BSA/RPMI medium. The migrated cells in the lower chamber were analyzed using FACS. The expression levels of monocyte CCR2 and CXCR4 were indicated by fluorescence intensities measured using FACS after staining with anti-CCR2-PE and anti-CXCR4-PE antibodies.

## 2.7. Immunofluorescence staining

Tumor tissues were isolated on day 28 after tumor inoculation, and the frozen tumor tissues were cut into 10-μm sections and mounted onto glass slides. Sections were fixed and permeabilized with cold acetone and blocked with 10% goat serum. To observe blood vessels and capillaries in tumor tissue, sections were incubated with anti-CD31 antibody (1:200, Sigma Aldrich) overnight at 4 °C, followed by incubation with the secondary antibody Alexa488 (1:200, Thermo Fisher Scientific). Immune cell density was analyzed by immunostaining; for the staining of immune cells, sections were incubated with respective antibodies, including CD4-PE, CD8-APC, CD19-PE, and F4/80-PE (1:100, BioLegend) after blocking. Images of blood vessels and immune cells were captured using an inverted fluorescence confocal microscope (LSM710, Carl Zeiss). A total of 25 images (5 × 5) of each sample were captured using the Tile scan mode to obtain a large view. The number of the anti-CD4/8, CD19, or F4/80 positive cells were counted over 100 cells from 3 different fields by image J software.

## 2.8. Quantitative real-time PCR

Total RNA was extracted from BMDMs using the TRIzol reagent (Thermo Fisher Scientific), according to the manufacturer's instructions. Reverse transcription of the extracted RNA was carried out using the PrimeScript™ RT reagent kit (Takara Bio, Otsu). The cDNA concentration was measured using a NanoDrop 2000 spectrophotometer. Quantitative RT-PCR was performed using the KOD SYBR qPCR Mix (TOYOBO Life Science) and StepOne Plus real-time PCR apparatus (Thermo Fisher Scientific). The PCR mixture included 2.5 μl cDNA, 1 μl primers, and 10 μl 2X Master Mix, and the program (98 °C for 10 s, 60 °C for 10 s, and 68 °C for 30 s) was set to 45 cycles. The expression of the housekeeping gene HPRT1 was used to normalize the qPCR results. The primers used are listed in Supplementary Table 1.

## 2.9. Lactate measurement

Lactate concentrations in medium and tissues or intracellular lactate levels in cells were assayed using a lactate assay kit (MAK064-1KT, Sigma Aldrich) according to the manufacturer's instructions and a microplate reader (SpectraMax i3x; Molecular Devices). Briefly, the cells or tissues were washed, homogenized, and lysed with RIPA buffer, and the supernatant was collected following centrifugation at 12,000×$g$ for 10 min. Fifty microliters of each sample or medium and standards was incubated with a 50 μl master mix (46 μl lactate assay buffer, 2 μl lactate enzyme mix, and 2 μl lactate probe) for 30 min at room temperature. The fluorescence intensity (ex = 535 nm/em = 587 nm) was measured. Lactate concentration was calculated according to the standard curve.

## 2.10. Lactate transport assay

To determine lactate permeability, intracellular pH was observed instead of measuring intracellular lactate levels directly, as described previously [34]. Cells in 96-well plates were treated as indicated, and stained with 2′,7′-Bis-(2-carboxyethyl)-5-(and-6)-carboxyfluorescein

(BCECF), a cell-permeant, dual-excitation ratiometric pH indicator, in which fluorescence decreases when the pH becomes more acidic. After incubation with BCECF for 30 min at 37 °C, the cells were washed and incubated with 100 μl Hanks' Balanced Salt Solution (HBSS). Fluorescence was measured using a microplate reader (SpectraMax i3x; Molecular Devices) after injection of 25 μl of lactate into each well. The continuous change in fluorescence within a 45 s window was recorded and fitted with a one-phase decay curve for comparison and analysis between different wells.

## 2.11. Statistical analyses

All data are expressed as means ± SEM. The statistical differences between groups were evaluated using an unpaired Student's $t$-test (two groups) or a one-way ANOVA followed by Tukey's multiple comparison test (when more than two groups were compared). P-values < 0.05 were considered statistically significant.

## 3. Results

### 3.1. Tumor progression in WT and AQP9$^{-/-}$ allograft tumor mouse model

To investigate tumor progression *in vivo*, MC38 cancer cells derived from colon adenocarcinoma were transplanted into the abdomen of male mice via subcutaneous injection, and continuous measurement of the tumor volume was carried out. As shown in Fig. 1A and B, tumor growth in AQP9$^{-/-}$ mice was suppressed compared to that observed in WT mice. Furthermore, the tumor weight of AQP9$^{-/-}$ mice was significantly lower than that of WT mice on day 28 (Fig. 1C). We observed the blood vessels via immunostaining of the tumor tissues with anti-CD31. Fig. 1D shows that the number of blood vessels was reduced in AQP9$^{-/-}$ mice compared with that observed in WT mice. Further, immunostaining of the tumor tissues with anti-F4/80 showed that the majority of macrophages were located in the region lacking blood vessels, which indicated that macrophages could promote angiogenesis in the tumor (Fig. 1D). These results indicate that tumor progression was suppressed by AQP9 knockout.

During tumor progression, the immune system can detect abnormal cell growth, and immune cells can infiltrate into the tumor environment [35]. We analyzed macrophage polarization in tumor tissues at day 28 using real-time PCR. Fig. 1E and F shows that the anti-tumor M1 macrophage polarization marker IFN-γ increased in AQP9$^{-/-}$ mice while TNF-α did not change significantly. Additionally, the mRNA levels of pro-tumor M2 macrophage polarization markers ARG1, CD163, and IL-10 were significantly decreased in AQP9$^{-/-}$ mice, while that of TGF-β showed no significant difference (Fig. 1G–J), which suggests that AQP9 deficiency reduced M2 macrophage polarization in the TME. Moreover, VEGF expression was decreased in AQP9$^{-/-}$ tissues, suggesting that AQP9$^{-/-}$ mice exhibited decreased tumor-associated angiogenesis (Fig. 1K). Taken together, these results demonstrate that AQP9-deficient mice are resistant to tumor progression in the tumor allograft model.

### 3.2. Reduced monocyte migration in the TME

Accumulated evidence has shown that during early development and progression of cancer, the innate and adaptive immune cells are of great importance in the TME [36–38]. To investigate early inflammation in tumor tissue, we analyzed the infiltrated immune cells in the TME on day 10 post transplantation using flow cytometry. Fig. 2A shows that the ratio of CD45$^+$-CD11b$^+$-ly6G$^-$-ly6C$^+$ monocytes was significantly reduced in AQP9$^{-/-}$ mice compared to that observed in WT mice (Fig. 2A), suggesting that AQP9$^{-/-}$ mice had fewer monocytes infiltrating into the TME. The ratio of MHCII$^+$ M1 macrophages and CD206$^+$ M2 macrophages was similar between WT and AQP9$^{-/-}$ mice (Supplementary Fig. S2A). The MFI of CD206 (marker of M2 polarization) was
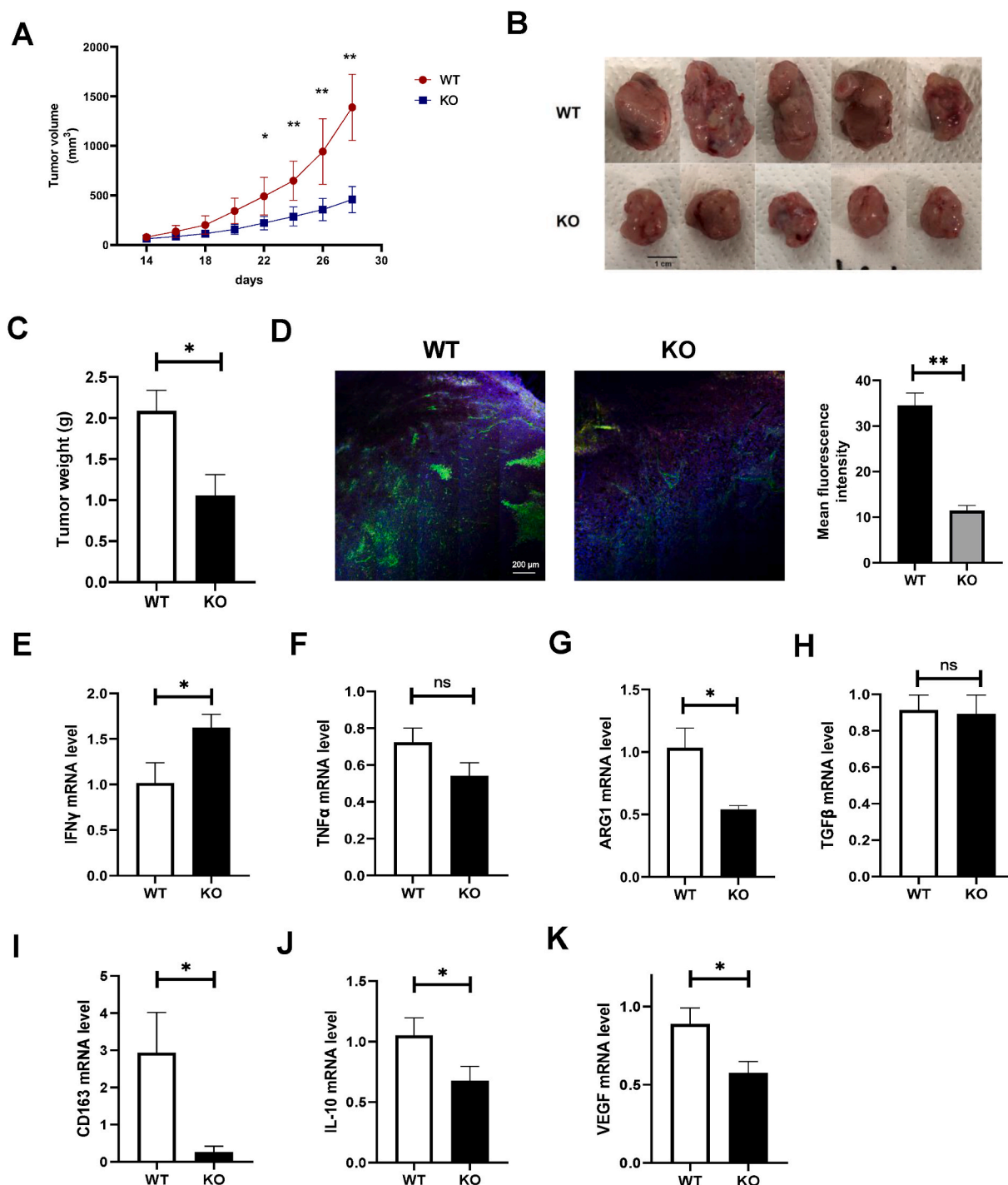
**Fig. 1.** AQP9$^{-/-}$ mice are resistant to tumor growth in a tumor allograft model

**A-D.** WT and AQP9$^{-/-}$ mice were subcutaneously injected with MC38 cells ($2 \times 10^5$ cells in 100 μl PBS) in the right flank. Mice were euthanized and tumor tissues were harvested on day 28 following injection. **A.** Tumor size was measured with a digital caliper every two days and the volume was calculated using the following formula: volume = (width × width × length)/2 (mean ± SE; n = 8 for WT and n = 6 for AQP9$^{-/-}$ mice; *$p < 0.05$, **$p < 0.01$). **B.** Representative images of tumors isolated from WT and AQP9$^{-/-}$ mice. **C.** Tumor weights for samples isolated from WT and AQP9$^{-/-}$ mice (mean ± SE; n = 6 for WT and n = 6 for AQP9$^{-/-}$ mice; *$p < 0.05$). **D.** (left) Immunostaining of tumor tissues with anti-CD31 (Alexa-488-green) and anti-F4/80 (PE-red). Bar = 200 μm. (right) Statistic graph of CD31 fluorescence intensity (mean ± SE; n = 3 for each group; **$p < 0.01$). **E-K.** mRNA expression of indicated genes in tumor tissue measured using RT-PCR and normalized to that of HPRT1 (mean ± SE; n = 4–6 for each group; *$p < 0.05$). Statistical analysis was performed using a two-tailed unpaired Student's *t*-test. Source data, including exact *p*-values, are provided in the Source Data file. (For interpretation of the references to colour in this figure legend, the reader is referred to the Web version of this article.)
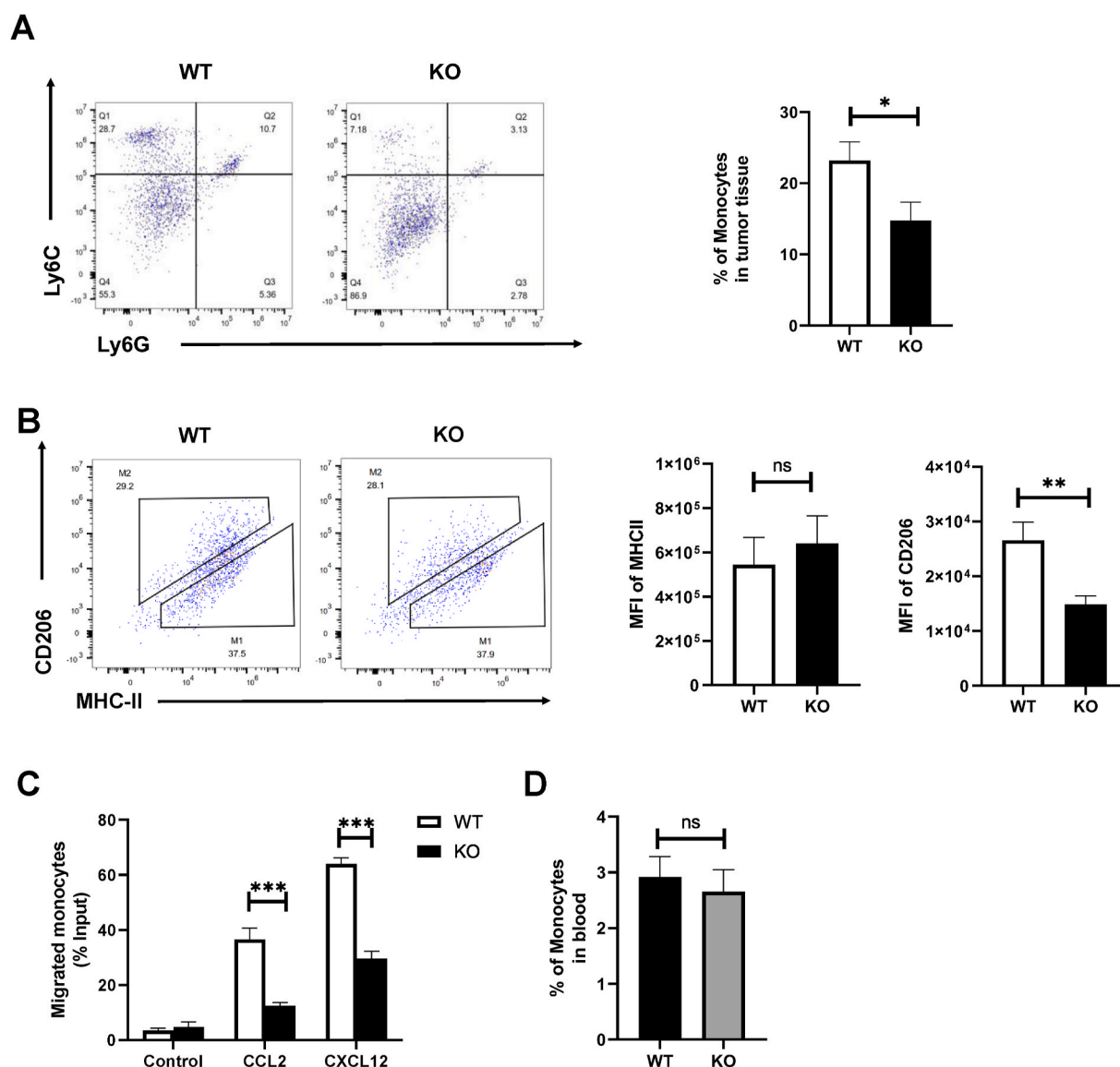
**Fig. 2.** Altered intratumoral monocyte and macrophage profile in AQP9$^{-/-}$ mice

**A.** Flow cytometry analysis of monocytes from the tumor microenvironment (left). Representative images of gating monocytes flow cytometry results of WT and AQP9$^{-/-}$ mice and (right) ratio (%) of monocytes (CD45$^+$ CD11b$^+$ Ly6G$^-$ Ly6C$^+$) in infiltrated immune cells (CD45$^+$ cells) (mean ± SE; n = 8–9 for each group; *$p <$ 0.05). **B.** Flow cytometry analysis of macrophages in tumor microenvironment (left). Representative images of gating M1/M2 macrophages flow cytometry results of WT and AQP9$^{-/-}$ mice and (right) MFI of MHCII and CD206 among CD45$^+$ CD11b$^+$ F4/80$^+$ cells (mean ± SE; n = 8–10 for each group; **$p <$ 0.01). **C.** Chemotaxis assay of monocytes toward CCL2 (20 ng/ml) and CXCL12 (100 ng/ml) for 2 h (n = 5; ***$p <$ 0.001). Cells were isolated from the bone marrow of WT and AQP9$^{-/-}$ mice. Cells migrated toward chemokines in a Transwell chamber, and the migrated monocytes (CD45$^+$ CD11b$^+$ Ly6G$^-$ Ly6C$^+$) were harvested and analyzed using FACS. **D.** Flow cytometry analysis of monocytes (CD45$^+$ CD11b$^+$ Ly6G$^-$ Ly6C$^+$) in blood (mean ± SE; n = 4 for each group; ns, no significance). Statistical analysis was performed using a two-tailed unpaired Student's *t*-test. Source data, including exact p-values, are provided in the Source Data file.

significantly decreased in the tumor tissue collected from AQP9$^{-/-}$ mice, whereas the MHCII (marker of M1 polarization) MFI was not significantly different between WT and AQP9$^{-/-}$ mice (as shown in Fig. 2B). We also tested the other infiltrated immune cells in the tumor, and the results showed no significant changes in CD4/8$^+$ T cells and CD19$^+$ B cells (Supplementary Fig. S2B). The total number of macrophages was comparable between WT and AQP9$^{-/-}$ tumor tissues (Supplementary Fig. S2C). This suggests that the M2-like polarization, and not proliferation, of macrophages was reduced in AQP9$^{-/-}$ mouse tumor, which may have contributed to the inhibition of tumor growth.

To examine the reason for the reduced number of monocytes infiltrated into the TME, a chemotaxis assay was performed to determine the migration of bone marrow monocytes. Monocytes from AQP9$^{-/-}$ mice exhibited decreased migration ability in response to CCL2 (20 ng/ml)

and CXCL12 (100 ng/ml) compared with those from WT mice, but they exhibited a similar density in blood (Fig. 2C and D). To exclude the influence of chemotaxis receptor expression, the expression levels of CCR2 and CXCR4 (receptors of CCL2 and CXCL12, respectively) were analyzed, and we observed similar expression levels in WT and AQP9$^{-/-}$ monocytes (Supplementary Fig. S2D). Taken together, these results indicate that during the early stage of tumor progression, fewer monocytes infiltrated into the TME due to the impaired migration function caused by AQP9 deficiency, and although the ratio of M1 and M2 macrophages was similar, the pro-tumoral M2-like polarization was reduced by AQP9-deficiency.

### 3.3. Suppressed M2-like polarization of AQP9-deficient macrophages by tumor-conditioned medium (TCM)

To investigate the mechanism underlying the reduced number of M2-type macrophages in the microenvironment, macrophage polarization was determined using BMDMs. BMDMs were stimulated with IFN-γ and LPS or IL-4 to stimulate M1 or M2 polarization. BMDMs were induced into M1 and M2 polarization states, as indicated by an increase in M1 markers (iNOS, TNF-α, and IL-6) or M2 markers (ARG1, CD206, and

Retnla); however, there were no significant changes between WT and AQP9$^{-/-}$ macrophages (Supplementary Figs. S3A–F).

Next, to further investigate the factors inducing M2 polarization within the TME, we collected TCM from MC38 cells, which represents a reliable and commonly used tool to study the TME products of cancer cells [16,39]. BMDMs were stimulated with TCM, and a subsequent mRNA analysis showed that the levels of the M1 polarization marker TNF-α significantly decreased while those of the M2 polarization markers ARG1, CD83, and VEGF significantly increased, suggesting that
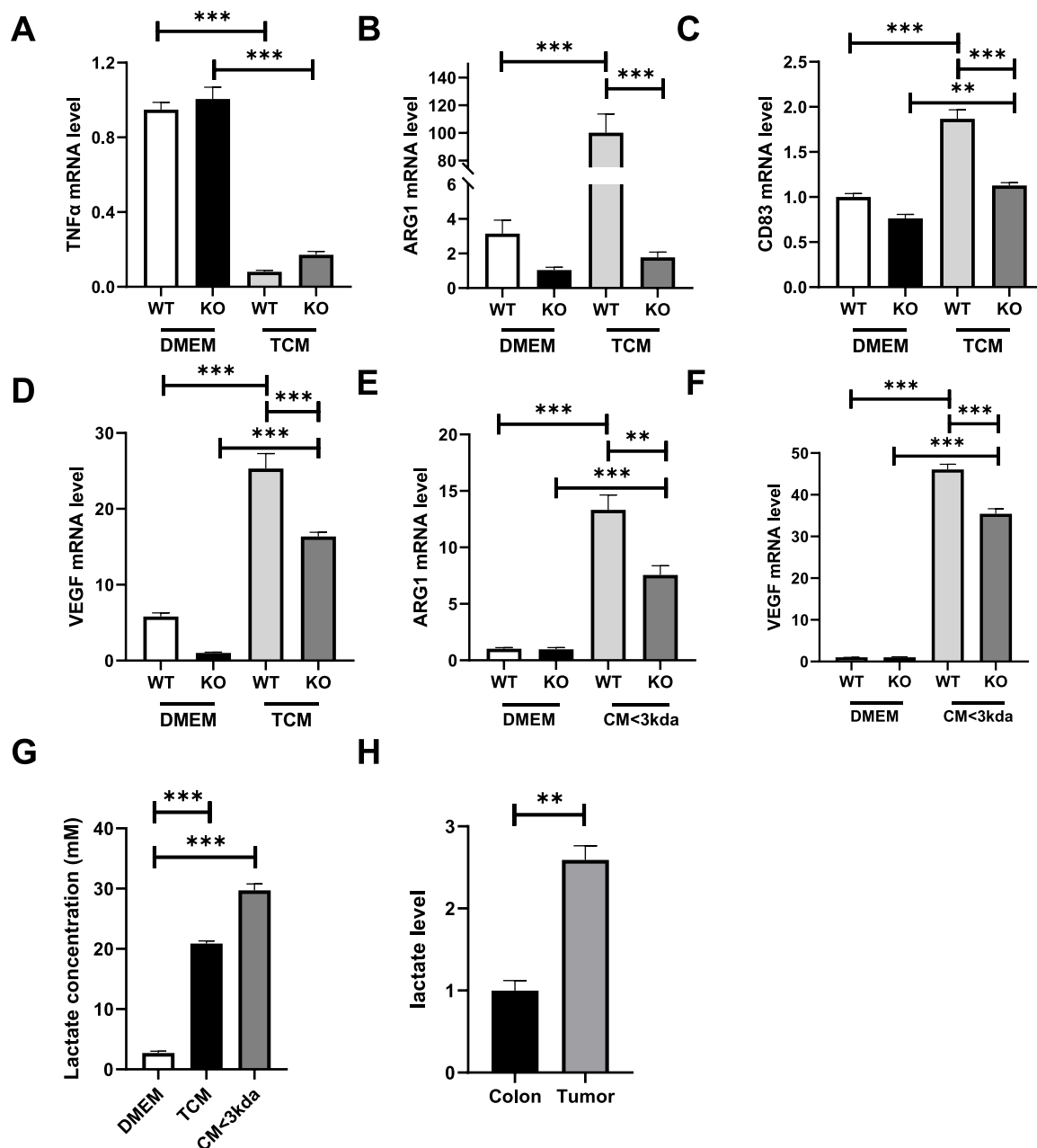


**Fig. 3.** Reduced tumor-conditioned medium (TCM)-induced M2-like polarization of AQP9$^{-/-}$ BMDMs
A-D. TCM was collected from MC38 cell culture medium after 2 days of incubation. BMDMs were treated with DMEM or TCM for 24 h. mRNA expression of *TNF-α, ARG1, CD83,* and *VEGF* in macrophages was analyzed using RT-PCR and normalized to that of HPRT1 (mean ± SE; n = 4 for each group; **$p < 0.01$, ***$p < 0.001$).
**E-F.** The <3 kDa fraction was separated from TCM using 3 kDa centrifugal filter. Macrophages were treated with DMEM or CM < 3 kDa for 24 h. mRNA expression of *ARG1* and *VEGF* in macrophages was analyzed using RT-PCR and normalized to that of HPRT1 (mean ± SE; n = 4 for each group; **$p < 0.01$, ***$p < 0.001$, ns, no significance). **G.** Lactate concentration in the medium (mean ± SE; n = 3–4 for each group; ***$p < 0.001$). **H.** Lactate level in the tissues (mean ± SE; n = 3 for each group; **$p < 0.01$). One-way ANOVA with Tukey's multiple comparison test or the two-tailed unpaired Student's *t*-test was used for the statistical analysis. Source data, including exact *p*-values, are provided in the Source Data file.

macrophages were polarized into M2-like macrophages (Fig. 3A–D). Although the expression level of TNF-α in BMDMs treated with TCM was not changed following AQP9 knockout (Fig. 3A), we observed a significant reduction in ARG1, CD83, and VEGF expression in AQP9$^{-/-}$ macrophages compared to that in WT BMDMs stimulated with TCM (Fig. 3B–D). Similar to the results from tumor tissue, the TGF-β expression did not change (Supplementary Fig. S3G). We observed the same phenotype of macrophages in the TME, indicating that AQP9 was related to the cancer cell products in the TME. Previous studies have shown that lactate secreted by cancer cells in TCM induces macrophage M2 polarization and plays a key role in tumor progression [16,17]. However, in our study, the M2-like polarization induced by TCM was reversed by

AQP9 deficiency. Therefore, to investigate whether the AQP9-related component of TCM was lactate, we further separated the TCM products using a 3 kDa filter and obtained a component of size of less than 3 kDa (CM < 3 kDa). Subsequently, the BMDMs were treated with the <3 kDa fraction. Fig. 3E shows that the <3 kDa fraction also induced an increase in ARG1 expression that was reduced by AQP9 deficiency. Similar results were observed in relation to TGF-β and VEGF mRNA levels following treatment with CM < 3 kDa (Fig. 3F and Supplementary S3H), the latter of which was repressed by AQP9 knockout (Fig. 3F). These results suggest that the M2-like polarization induced by TCM components from the <3 kDa fraction was significantly blocked by AQP9 deficiency. We hypothesize that lactate might be the TCM
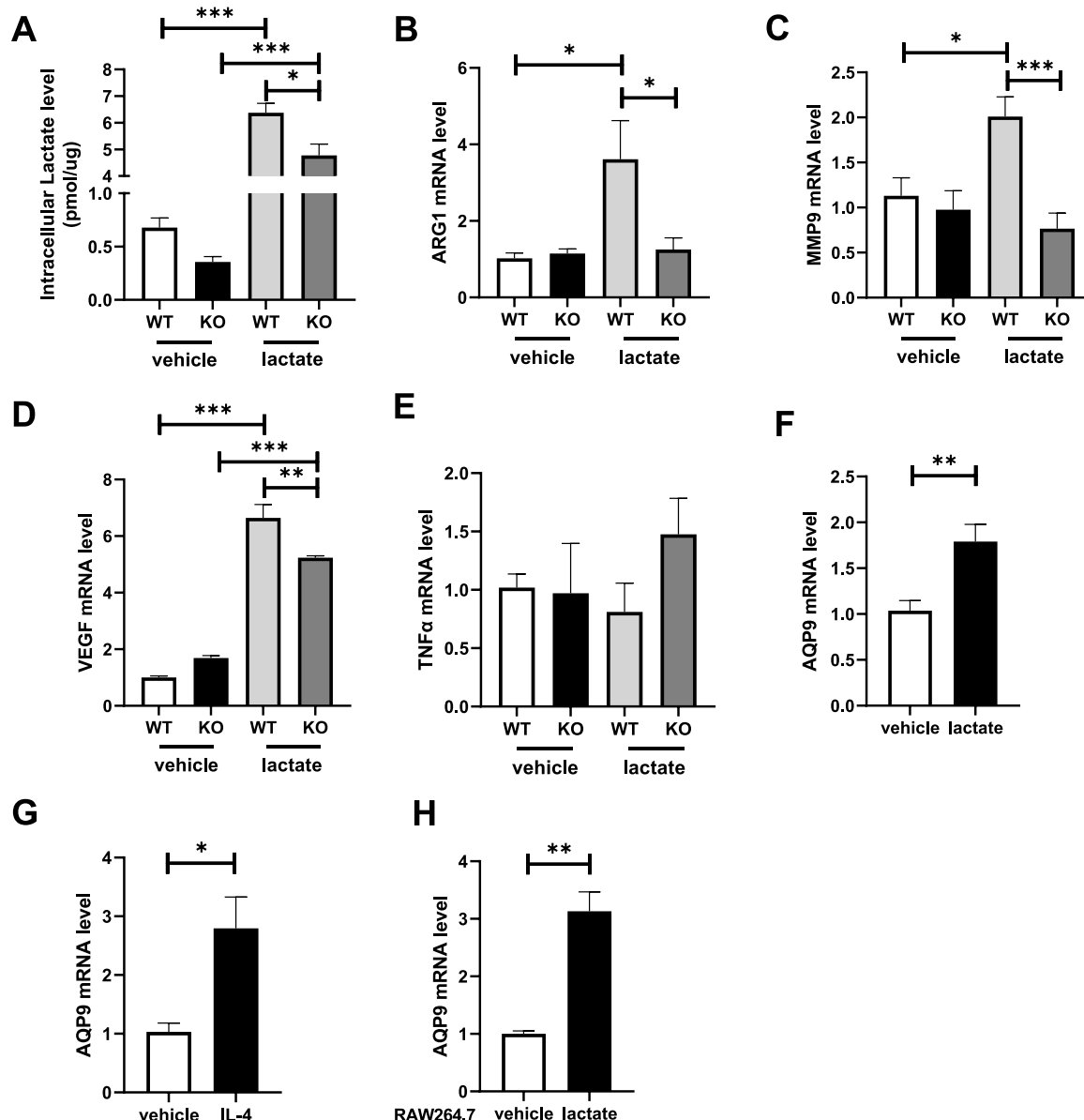


**Fig. 4.** Suppressed lactate-induced M2-like polarization in AQP9$^{-/-}$ BMDMs
**A-F.** BMDMs were treated with vehicle or 25 mM lactate for 12 h. **A.** Intracellular lactate level (mean ± SE; n = 3 for each group; *$p < 0.05$, ***$p < 0.001$). **B-E.** mRNA expression of indicated genes in BMDMs measured using RT-PCR and normalized to that of HPRT1 (mean ± SE; n = 4–8 for each group; *$p < 0.05$, **$p < 0.01$, ***$p < 0.001$). **F–H.** AQP9 mRNA expression in macrophages was analyzed using RT-PCR and normalized to that of HPRT1. **F.** BMDMs were treated with vehicle or 25 mM lactate (mean ± SE; n = 7 for vehicle and 8 for lactate group; **$p < 0.01$). **G.** BMDMs were treated with vehicle or IL-4 (mean ± SE; n = 4 for each group; *$p < 0.05$). **H.** RAW264.7 macrophages were treated with vehicle or 25 mM lactate (mean ± SE; n = 4 for each group; **$p < 0.01$). Statistical analysis was performed using a one-way ANOVA with Tukey's multiple comparison test or the two-tailed unpaired Student's $t$-test. Source data, including exact $p$-values, are provided in the Source Data file.

component secreted by cancer cells that was affected by AQP9 deficiency. Therefore, we measured the lactate in fresh medium (DMEM), TCM, and CM < 3 kDa. We discovered that TCM and CM < 3 kDa had a significantly higher concentration of lactate (more than 21 mM) than fresh DMEM (Fig. 3G). Similar results were obtained from tissues where carcinoma cells had a higher concentration of lactate than did normal colon tissue (Fig. 3H). Because of the Warburg-effect, carcinoma cells tend to convert most glucose to lactate using glycolysis, which has been considered as a hallmark of cancer metabolism switch, while normal cells do not [40,41]. These results suggest that lactate plays a role in tumor progression.

### 3.4. Reduced lactate-induced M2-like polarization in AQP9$^{-/-}$ macrophages

To determine the relationship between lactate and AQP9 in macrophages, we treated BMDMs with lactate and examined the polarization. First, we measured intracellular lactate concentration of macrophages. As shown in Fig. 4A, the concentration of lactate was significantly higher in WT than in AQP9$^{-/-}$ macrophages treated with lactate, indicating the involvement of AQP9 in the regulation of intracellular lactate. Next, we investigated the expression of the M2 polarization markers. The expression of M2 markers, ARG1 and MMP9, was increased by lactate treatment, while AQP9 knockout resulted in a significant reduction (Fig. 4B and C). In line with our previous results, TGF-β levels did not change between WT and AQP9$^{-/-}$ mice (Supplementary Fig. S3I). Moreover, VEGF expression was increased following lactate stimulation and the elevation was suppressed by AQP9 deficiency (Fig. 4D).

Alternatively, the M1 marker TNF-α was not affected by lactate treatment (Fig. 4E). These results indicated that lactate-induced M2-like macrophage polarization was attenuated by AQP9 deficiency. A previous study performed a microarray analysis in mouse M2 macrophages and showed that AQP9 is upregulated in these cells, which allows us to interpret the potential effect of lactate treatment on AQP9 expression [42]. Furthermore, we performed real-time PCR to measure AQP9 expression in macrophages. Similar to the previous report, AQP9 expression was promoted by both lactate and IL-4 treatments of primary culture macrophages (Fig. 4F and G). The RAW264.7 macrophage cell line had an increased AQP9 expression level in response to lactate treatment as well (Fig. 4H). Taken together, our results suggest that AQP9 plays an essential role in regulating lactate-induced macrophage M2-like polarization in vivo and in vitro.

### 3.5. Involvement of AQP9 expression in lactate transport in macrophages

Previous studies have shown that AQP9 is capable of lactate transport using Xenopus oocytes [43,44] and yeast cells [45,46]; however, this has not been determined in mammalian cells. We thus examined whether AQP9 could transport lactate into mouse macrophages. First, an AQP9-overexpressing Chinese hamster ovary cell line (AQP9-CHO cells, shown in Supplementary Figs. S4B and S4C) was established to confirm the involvement of AQP9 in lactate transport. We confirmed that AQP9 overexpression increased water permeability (Supplementary Fig. S4D), suggesting that this cell line could be used to detect the AQP9 transport function. The pH-dependent dye 2′,7′-Bis-(2-carboxyethyl)-5-(and-6)-carboxyfluorescein (BCECF), lower fluorescence
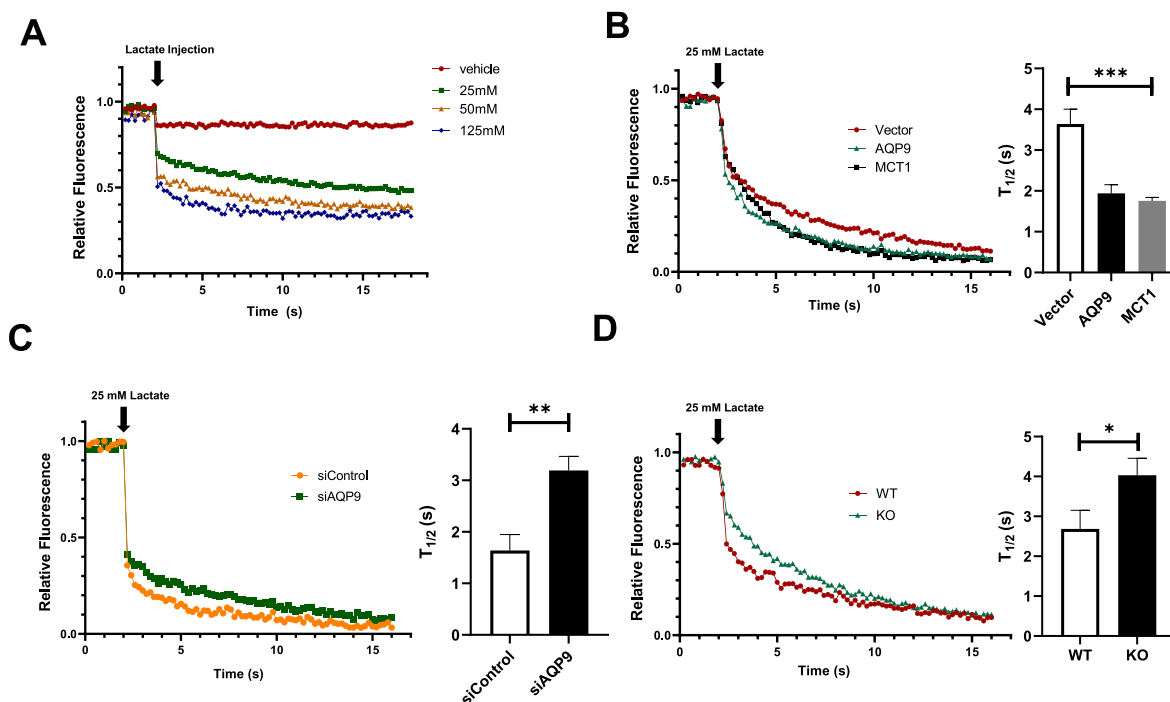


**Fig. 5.** Lactate transport through AQP9 in macrophages
**A-D.** The lactate permeability of cells was measured based on the time course of the pH-sensitive dye BCECF fluorescence in response to lactate gradients at 23 °C. Low fluorescence indicates low intracellular pH. **A-B.** AQP9-overexpressing CHO cell line (AQP9-CHO cell) was established by transfecting the pCMV6-AQP9 plasmid into naïve CHO cells. **A.** Representative time-course data showing AQP9-CHO cell responses to rapid changes in intracellular pH caused by different concentrations of lactate (vehicle, 25, 50, and 125 mM). **B.** (left) Representative time-course data showing CHO cell (transfected with empty-vector, pCMV6-AQP9, or pCMV6-MCT1) responses to rapid changes in intracellular pH caused by 25 mM lactate (right). Averaged decreasing curve parameter $T_{1/2}$ (mean ± SE, n = 6 for each group, *$p <$ 0.05). **C.** (left) Representative time-course data showing the responses of RAW264.7 cells transfected with si-control or si-AQP9 to rapid changes in intracellular pH caused by 25 mM lactate. (right) Averaged curve parameter $T_{1/2}$ (mean ± SE; n = 5 for each group; **$p <$ 0.01). **D.** (left) Representative time-course data showing WT and AQP9$^{-/-}$ macrophage responses to rapid changes in intracellular pH caused by 25 mM lactate. (right) Averaged $T_{1/2}$ (mean ± SE; n = 12 for WT and n = 10 for AQP9$^{-/-}$ group; *$p <$ 0.05). Statistical analysis was performed using a two-tailed unpaired Student's t-test. Source data, including exact p-values, are provided in the Source Data file.

indicated lower pH) was used to analyze lactate permeability, as described previously [34]. AQP9-CHO cells were loaded with BCECF and incubated with different concentrations of lactate. As shown in Fig. 5A, the fluorescence decreased faster in AQP9-CHO cells under lactate treatment than in the vehicle. In addition, the decrease in fluorescence (pH) was lactate dose-dependent, suggesting that the lactate transport assay was reliable for the CHO cell line. There are two well-known lactate transporters in mammalian cells, namely monocarboxylate transporter (MCT) 1 and 4 [47]. We confirmed that both MCT1 and MCT4 were expressed in WT and AQP9$^{-/-}$macrophages (Supplementary Fig. S4A). Therefore, we established an MCT1-overexpressing CHO cell line (Supplementary Fig. S4E) and examined the lactate transport in CHO cells with a vector, AQP9, and MCT1 by adding 25 mM lactate. The obtained data points were fitted into a one-phase decay curve, and the 'T$_{1/2}$' parameter was calculated to indicate the rate of fluorescence decrease. AQP9-CHO cells had a faster fluorescence decay curve, and the T$_{1/2}$ was significantly lower in AQP9-CHO cells than in CHO cells with the vector and was similar to that observed MCT1-CHO cells. This suggests that AQP9 may play important roles in lactate permeability (Fig. 5B). To further verify the involvement of AQP9 in macrophage lactate transport, we used RAW264.7 cells transfected with si-AQP9 (Supplementary Fig. S4F). AQP9 knockdown RAW264.7 cells showed a slower fluorescence decrease rate with a significantly increased T$_{1/2}$ compared with that of the control siRNA-transfected cells (Fig. 5C). This indicates that the transport of lactate was reduced by AQP9 knockdown. Furthermore, the T$_{1/2}$ in AQP9$^{-/-}$ BMDMs was significantly higher than that observed in WT BMDMs (Fig. 5D); thus, indicating that AQP9 deficiency affected the lactate permeability of BMDMs. Taken together, these results demonstrate that AQP9 is involved in macrophage lactate transport.

In summary, our findings suggest that AQP9 functions as a lactate transporter in macrophages, and AQP9$^{-/-}$ mice were resistant to tumor growth due to the reduced macrophage M2-like polarization, which was caused by a blockage of lactate transport (Supplementary Fig. S5).

## 4. Discussion

Here, we showed that AQP9-deficient mice were resistant to tumor growth. First, AQP9$^{-/-}$ mice showed suppressed tumor growth in an allograft tumor model. Macrophage M2-like polarization in the tumor was reduced, and monocyte chemotaxis was impaired, in AQP9$^{-/-}$ mice, indicating that the pro-tumor immunity was suppressed in these mice. Second, treatment of TCM with BMDMs induced M2-like polarization; however, this effect and induction of VEGF expression were reversed by AQP9 deficiency. Furthermore, AQP9 deficiency was associated with impaired induction of M2-like polarization following stimulation with the <3 kDa fraction. This suggests that AQP9 is involved in cancer cell product-induced macrophage M2-like polarization. More specifically, lactate addition induced M2-like polarization in BMDMs, which was also blocked by AQP9 deficiency, indicating that AQP9 may play a role in transporting lactate into macrophages. Third, AQP9 overexpression in CHO cells showed enhanced lactate permeability, which was attenuated by AQP9 knockdown and knockout, suggesting that AQP9 had a lactate-transporting function in macrophages. Collectively, these results support that AQP9 enhances lactate uptake and M2-like macrophage polarization, which contributes to cancer progression, and that AQP9 deficiency had the opposite effects.

Macrophages are the innate and adaptive immune cells that differentiate from monocytes or are recruited to the tumor site by chemokines [48]. Recent studies have reported that reducing M2 polarization or shifting toward M1 activation significantly suppresses tumor growth and metastasis [49,50]. In this study, we revealed the role of AQP9 in TME macrophage polarization and showed that AQP9$^{-/-}$ mice exhibited suppressed tumor progression due to the reduced M2-like polarization. Moreover, previous studies have demonstrated that TAMs, especially the M2-like phenotype, drive cancer progression by secreting several

factors, such as IL-6, IL-8, and IL-10 [51–53]. In the current study, we showed that the expression of M2 markers, such as ARG1, CD163, and IL-10, was decreased in AQP9$^{-/-}$ tumor tissues. Additionally, TAMs secrete collagenase-like matrix metallopeptidase-9 (MMP9) to promote angiogenesis, tumor invasion, and further recruitment of TAMs [52,54], and our in vitro experiments using BMDMs treated with lactate showed increased MMP9 expression, which was reversed by AQP9 deficiency. These results indicate that AQP9 contributes to promote macrophage M2-like polarization and tumor suppression.

Lactate, which is excessively produced by cancer cells in the TME, can be taken up by macrophages and used to induce the expression of M2-like genes, which are key factors in remodeling and immune suppression [55,56]. Oscar et al. first demonstrated that lactate produced by tumor cells induces M2 macrophage polarization and VEGF expression, which in turn aggravates tumor progression and promotes angiogenesis [16]. In this study, BMDMs treated with lactate (25 mM) exhibited an increased expression of the M2 marker, ARG1, and the expression of VEGF, both of which were suppressed by AQP9 deficiency, indicating that AQP9 was involved in the lactate-M2 macrophage pathway. However, the mechanism underlying M2 polarization induced by lactate has not been elucidated. Mu et al. reported that lactate-induced M2 macrophage polarization might rely on the ERK/STAT3 pathway [17]. In addition, Zhang et al. found a new histone modification called 'lactylation' and revealed that lactate plays a role in gene transcription regulation in macrophages. The lactate transported into cells modified histone 3 lysine residues and upregulated the M2-like macrophage gene Arg*1* [57]. In our study, we found a new route of lactate uptake in macrophages via AQP9. However, further studies are warranted to understand the mechanism by which lactate regulates the M2-like polarization pathway in macrophages after the import of lactate.

Concurrent with our findings, recent studies have illustrated that AQP9 expression can be used as a prognostic indicator in patients with cancer. AQP9 was found to be upregulated in RCC and its expression could be used for diagnosis and prognosis prediction, and it is a potential therapeutic target [58]. In addition, an integrated analysis using several cancer databases reported that AQP9 was highly expressed in several cancer types and was identified as a prognosticator in multiple cancers. Furthermore, high AQP9 expression was shown to be associated with the immune-infiltrating levels [59]. Moreover, a recent study found that AQP9 expression was positively correlated with M2 TAMs in kidney cancer, and AQP9 expression might be helpful in predicting patient prognosis [60]. In our study, we found that the loss of AQP9 expression was beneficial for tumor resistance through the inhibition of the M2-like polarization in the TME. Thus, AQP9 might represent a potential target for anti-cancer treatment.

Aquaporins are integral membrane transport proteins, whose primary function is to facilitate water permeability. However, AQP9 was also reported to transport other small solutes [61]. Urea and glycerol were first discovered to be permeable by AQP9 in rats [43]. Further, human AQP9 was reported to enable the transport of arsenite, monomethyselenic acid, selenite, and silicon [44,62,63]. In addition, AQP9 was shown to uptake lactate when expressed in oocytes, and Rothert et al. confirmed the lactate transport function of human AQP9 overexpressed in yeast cells [43,46]. In our study, based on the reported small solute permeability of AQP9, we determined that AQP9 exhibits a lactate transport function in macrophages. By using the pH-sensitive dye, BCECF, we showed that AQP9 overexpression CHO cells had faster lactate transport and that si-AQP9 and AQP9 knockout can block lactate transport in macrophages. Thus, we identified a new route for lactate transport in mammalian cells, which could be used as a potential immune therapy target for anti-tumor treatment.

## 5. Conclusion

In summary, our data demonstrated a novel lactate transport function of AQP9 and interpreted its role in the polarization of TAMs.

Furthermore, our findings support that AQP9 is a novel target for TAM-related pro-tumoral effects by regulating lactate transport in the TME.

## Data availability

All data are included in this manuscript (and its supplementary information files).

## Author contributions

Y.S. and M.H.-C. conceptualization; Y.S. and M.H.-C. methodology; Y.S. and M.H.-C. formal analysis; Y.S. investigation, data curation, writing–original draft; M.H.-C. review and editing; M.H.-C. and M.Y. supervision.

## Funding and additional information

## Declaration of competing interest

The authors declare that they have no known competing financial interests or personal relationships that could have appeared to influence the work reported in this paper.

## Acknowledgments

## Appendix A. Supplementary data

Supplementary data to this article can be found online at https://doi.org/10.1016/j.bbrep.2022.101317.

## References

[1] H. Sung, J. Ferlay, R.L. Siegel, M. Laversanne, I. Soerjomataram, A. Jemal, F. Bray, Global cancer statistics 2020: GLOBOCAN estimates of incidence and mortality worldwide for 36 cancers in 185 countries, Ca-a Cancer Journal for Clinicians 71 (2021) 209–249, https://doi.org/10.3322/caac.21660.

[2] F. Arvelo, F. Sojo, C. Cotte, Biology of colorectal cancer, Ecancermedicalscience 9 (2015), https://doi.org/10.3332/ecancer.2015.520.

[3] A. Sveen, S. Kopetz, R.A. Lothe, Biomarker-guided therapy for colorectal cancer: strength in complexity, Nat. Rev. Clin. Oncol. 17 (2020) 11–32, https://doi.org/10.1038/s41571-019-0241-1.

[4] D. Rosenblum, N. Joshi, W. Tao, J.M. Karp, D. Peer, Progress and challenges towards targeted delivery of cancer therapeutics, Nat. Commun. 9 (2018), https://doi.org/10.1038/s41467-018-03705-y.

[5] V.G. Peddareddigari, D. Wang, R.N. Dubois, The tumor microenvironment in colorectal carcinogenesis, Cancer Microenviron 3 (2010) 149–166, https://doi.org/10.1007/s12307-010-0038-3.

[6] C. Murdoch, M. Muthana, S.B. Coffelt, C.E. Lewis, The role of myeloid cells in the promotion of tumour angiogenesis, Nat. Rev. Cancer 8 (2008) 618–631, https://doi.org/10.1038/nrc2444.

[7] R.A. Franklin, W. Liao, A. Sarkar, M.V. Kim, M.R. Bivona, K. Liu, E.G. Pamer, M. O. Li, The cellular and molecular origin of tumor-associated macrophages, Science 344 (2014) 921–925, https://doi.org/10.1126/science.1252510.

[8] Y.H. Wang, C.Y. Shen, S.C. Lin, W.H. Kuo, Y.T. Kuo, Y.L. Hsu, W.C. Wang, K.T. Lin, L.H. Wang, Monocytes secrete CXCL7 to promote breast cancer progression, Cell Death Dis. 12 (2021) 1090, https://doi.org/10.1038/s41419-021-04231-4.

[9] C.E. Olingy, H.Q. Dinh, C.C. Hedrick, Monocyte heterogeneity and functions in cancer, J. Leukoc. Biol. 106 (2019) 309–322, https://doi.org/10.1002/JLB.4RI0818-311R.

[10] M. Erreni, A. Mantovani, P. Allavena, Tumor-associated macrophages (TAM) and inflammation in colorectal cancer, Cancer Microenviron 4 (2011) 141–154, https://doi.org/10.1007/s12307-010-0052-5.

[11] A.J. Petty, Y. Yang, Tumor-associated macrophages: implications in cancer immunotherapy, Immunotherapy 9 (2017) 289–302, https://doi.org/10.2217/imt-2016-0135.

[12] Z.C. He, S.X. Zhang, Tumor-associated macrophages and their functional transformation in the hypoxic tumor microenvironment, Front. Immunol. 12 (2021) 11, https://doi.org/10.3389/fimmu.2021.741305.

[13] J.Y. Liu, X.F. Geng, J.X. Hou, G.S. Wu, New insights into M1/M2 macrophages: key modulators in cancer progression, Cancer Cell Int. 21 (2021) 7, https://doi.org/10.1186/s12935-021-02089-2.

[14] T. Colangelo, G. Polcaro, L. Muccillo, G. D'Agostino, V. Rosato, P. Ziccardi, A. Lupo, G. Mazzoccoli, L. Sabatino, V. Colantuoni, Friend or foe? The tumour microenvironment dilemma in colorectal cancer, Biochimica Et Biophysica Acta-Reviews on Cancer 1867 (2017) 1–18, https://doi.org/10.1016/j.bbcan.2016.11.001.

[15] Z.H. Wang, W.B. Peng, P. Zhang, X.P. Yang, Q. Zhou, Lactate in the tumour microenvironment: from immune modulation to therapy, EBioMedicine 73 (2021) 9, https://doi.org/10.1016/j.ebiom.2021.103627.

[16] O.R. Colegio, N.Q. Chu, A.L. Szabo, T. Chu, A.M. Rhebergen, V. Jairam, N. Cyrus, C.E. Brokowski, S.C. Eisenbarth, G.M. Phillips, et al., Functional polarization of tumour-associated macrophages by tumour-derived lactic acid, Nature 513 (2014) 559, https://doi.org/10.1038/nature13490.

[17] X.M. Mu, W. Shi, Y. Xu, C. Xu, T. Zhao, B. Geng, J. Yang, J.S. Pan, S. Hu, C. Zhang, et al., Tumor-derived lactate induces M2 macrophage polarization via the activation of the ERK/STAT3 signaling pathway in breast cancer, Cell Cycle 17 (2018) 428–438, https://doi.org/10.1080/15384101.2018.1444305.

[18] P.W. Chen, H. Zuo, H. Xiong, M.J. Kolar, Q. Chu, A. Saghatelian, D.J. Siegwart, Y. H. Wan, Gpr132 sensing of lactate mediates tumor-macrophage interplay to promote breast cancer metastasis, in: Proceedings of the National Academy of Sciences of the United States of America, vol. 114, 2017, pp. 580–585, https://doi.org/10.1073/pnas.1614035114.

[19] N. Liu, J. Luo, D. Kuang, S. Xu, Y. Duan, Y. Xia, Z. Wei, X. Xie, B. Yin, F. Chen, et al., Lactate inhibits ATP6V0d2 expression in tumor-associated macrophages to promote HIF-2α-mediated tumor progression, J. Clin. Invest. 129 (2019) 631–646, https://doi.org/10.1172/JCI123027.

[20] A.S. Verkman, Aquaporins. Current Biology 23 (2013) R52–R55, https://doi.org/10.1016/j.cub.2012.11.025.

[21] Y.J. Liu, D. Promeneur, A. Rojek, N. Kumar, J. Frokiaer, S. Nielsen, L.S. King, P. Agre, J.M. Carbrey, Aquaporin 9 is the major pathway for glycerol uptake by mouse erythrocytes, with implications for malarial virulence, in: Proceedings of the National Academy of Sciences of the United States of America, vol. 104, 2007, pp. 12560–12564, https://doi.org/10.1073/pnas.0705313104.

[22] S. Watanabe, C.S. Moniaga, S. Nielsen, M. Hara-Chikuma, Aquaporin-9 facilitates membrane transport of hydrogen peroxide in mammalian cells, Biochem. Biophys. Res. Commun. 471 (2016) 191–197, https://doi.org/10.1016/j.bbrc.2016.01.153.

[23] N. Maeda, T. Funahashi, F. Shimomura, Metabolic impact of adipose and hepatic glycerol channels aquaporin 7 and aquaporin 9, Nat. Clin. Pract. Endocrinol. Metabol. 4 (2008) 627–634, https://doi.org/10.1038/ncpendmet0980.

[24] T. Karlsson, M. Glogauer, R.P. Ellen, V.M. Loitto, K.E. Magnusson, M.A. O. Magalhaes, Aquaporin 9 phosphorylation mediates membrane localization and neutrophil polarization, J. Leukoc. Biol. 90 (2011) 963–973, https://doi.org/10.1189/jlb.0910540.

[25] A. Holm, K.E. Magnusson, E. Vikstrom, Pseudomonas aeruginosa N-3-oxo-dodecanoyl-homoserine lactone elicits changes in cell volume, morphology, and AQP9 characteristics in macrophages, Front. Cell. Infect. Microbiol. 6 (2016) 15, https://doi.org/10.3389/fcimb.2016.00032.

[26] C.S. Moniaga, S. Watanabe, T. Honda, S. Nielsen, M. Hara-Chikuma, Aquaporin-9-expressing neutrophils are required for the establishment of contact hypersensitivity, Sci. Rep. 5 (2015), 15319, https://doi.org/10.1038/srep15319.

[27] W.H. Xu, S.N. Shi, Y. Xu, J. Wang, H.K. Wang, D.L. Cao, G.H. Shi, Y.Y. Qu, H. L. Zhang, D.W. Ye, Prognostic implications of Aquaporin 9 expression in clear cell renal cell carcinoma, J. Transl. Med. 17 (2019) 14, https://doi.org/10.1186/s12967-019-2113-y.

[28] L.Z. Zhu, N. Ma, B. Wang, L. Wang, C. Zhou, Y. Yan, J.J. He, Y. Ren, Significant prognostic values of aquaporin mRNA expression in breast cancer, Cancer Manag. Res. 11 (2019) 1503–1515, https://doi.org/10.2147/cmar.s193396.

[29] Y. Yamada, T. Arai, M. Kato, S. Kojima, S. Sakamoto, A. Komiya, Y. Naya, T. Ichikawa, N. Seki, Role of pre-miR-532 (miR-532-5p and miR-532-3p) in regulation of gene expression and molecular pathogenesis in renal cell carcinoma, American Journal of Clinical and Experimental Urology 7 (2019) 11–30.

[30] C.J. Liu, F.F. Hu, M.X. Xia, L. Han, Q. Zhang, A.Y. Guo, GSCALite: a web server for gene set cancer analysis, Bioinformatics 34 (2018) 3771–3772, https://doi.org/10.1093/bioinformatics/bty411.

[31] A.M. Rojek, M.T. Skowronski, E.M. Füchtbauer, A.C. Füchtbauer, R.A. Fenton, P. Agre, J. Frøkiaer, S. Nielsen, Defective glycerol metabolism in aquaporin 9 (AQP9) knockout mice, Proc. Natl. Acad. Sci. U. S. A. 104 (2007) 3609–3614, https://doi.org/10.1073/pnas.0610894104.

[32] M.M. Jensen, J.T. Jørgensen, T. Binderup, A. Kjaer, Tumor volume in subcutaneous mouse xenografts measured by microCT is more accurate and reproducible than determined by 18F-FDG-microPET or external caliper, BMC Med. Imag. 8 (2008) 16, https://doi.org/10.1186/1471-2342-8-16.

[33] M. Hara-Chikuma, M. Tanaka, A.S. Verkman, M. Yasui, Inhibition of aquaporin-3 in macrophages by a monoclonal antibody as potential therapy for liver injury, Nat. Commun. 11 (2020) 5666, https://doi.org/10.1038/s41467-020-19491-5.

[34] C.M. Murray, R. Hutchinson, J.R. Bantick, G.P. Belfield, A.D. Benjamin, D. Brazma, R.V. Bundick, I.D. Cook, R.I. Craggs, S. Edwards, et al., Monocarboxylate

transporter MCT1 is a target for immunosuppression, Nat. Chem. Biol. 1 (2005) 371–376, https://doi.org/10.1038/nchembio744.

[35] H. Gonzalez, C. Hagerling, Z. Werb, Roles of the immune system in cancer: from tumor initiation to metastatic progression, Genes Dev. 32 (2018) 1267–1284, https://doi.org/10.1101/gad.314617.118.

[36] D. Mittal, M.M. Gubin, R.D. Schreiber, M.J. Smyth, New insights into cancer immunoediting and its three component phases–elimination, equilibrium and escape, Curr. Opin. Immunol. 27 (2014) 16–25, https://doi.org/10.1016/j.coi.2014.01.004.

[37] L. Corrales, V. Matson, B. Flood, S. Spranger, T.F. Gajewski, Innate immune signaling and regulation in cancer immunotherapy, Cell Res. 27 (2017) 96–108, https://doi.org/10.1038/cr.2016.149.

[38] C. Hagerling, A.J. Casbon, Z. Werb, Balancing the innate immune system in tumor development, Trends Cell Biol. 25 (2015) 214–220, https://doi.org/10.1016/j.tcb.2014.11.001.

[39] L. Tóth, G. Pásti, A. Sárváry, M. Balázs, R. Adány, Effect of tumor-conditioned medium on intercellular communication and proliferation of Balb/c 3T3 cells, Cancer Lett. 151 (2000) 57–61, https://doi.org/10.1016/s0304-3835(99)00403-6.

[40] D. Hanahan, R.A. Weinberg, Hallmarks of cancer: the next generation, Cell 144 (2011) 646–674, https://doi.org/10.1016/j.cell.2011.02.013.

[41] S. Devic, Warburg effect - a consequence or the cause of carcinogenesis? J. Cancer 7 (2016) 817–822, https://doi.org/10.7150/jca.14274.

[42] K.A. Jablonski, S.A. Amici, L.M. Webb, JeD. Ruiz-Rosado, P.G. Popovich, S. Partida-Sanchez, M. Guerau-de-Arellano, Novel markers to delineate murine M1 and M2 macrophages, PLoS One 10 (2015), e0145342, https://doi.org/10.1371/journal.pone.0145342.

[43] H. Tsukaguchi, C. Shayakul, U.V. Berger, B. Mackenzie, S. Devidas, W.B. Guggino, A.N. van Hoek, M.A. Hediger, Molecular characterization of a broad selectivity neutral solute channel, J. Biol. Chem. 273 (1998) 24737–24743, https://doi.org/10.1074/jbc.273.38.24737.

[44] X. Geng, J. McDermott, J. Lundgren, L. Liu, K.J. Tsai, J. Shen, Z. Liu, Role of AQP9 in transport of monomethyselenic acid and selenite, Biometals 30 (2017) 747–755, https://doi.org/10.1007/s10534-017-0042-x.

[45] A. Bader, E. Beitz, Transmembrane facilitation of lactate/H. Membranes, Baseline 10 (2020), https://doi.org/10.3390/membranes10090236.

[46] M. Rothert, D. Rönfeldt, E. Beitz, Electrostatic attraction of weak monoacid anions increases probability for protonation and passage through aquaporins, J. Biol. Chem. 292 (2017) 9358–9364, https://doi.org/10.1074/jbc.M117.782516.

[47] A. Bonen, The expression of lactate transporters (MCT1 and MCT4) in heart and muscle, Eur. J. Appl. Physiol. 86 (2001) 6–11, https://doi.org/10.1007/s004210100516.

[48] T. Keeley, D.L. Costanzo-Garvey, L.M. Cook, Unmasking the many faces of tumor-associated neutrophils and macrophages: considerations for targeting innate immune cells in cancer, Trends Cancer 5 (2019) 789–798, https://doi.org/10.1016/j.trecan.2019.10.013.

[49] A. Sui, X. Chen, A.M. Demetriades, J. Shen, Y. Cai, Y. Yao, Y. Zhu, X. Shen, B. Xie, Inhibiting NF-κB signaling activation reduces retinal neovascularization by promoting a polarization shift in macrophages, Invest. Ophthalmol. Vis. Sci. 61 (2020) 4, https://doi.org/10.1167/iovs.61.6.4.

[50] R.S. Cavalcante, U. Ishikawa, E.S. Silva, A.A. Silva-Júnior, A.A. Araújo, L.J. Cruz, A.B. Chan, R.F. de Araújo Júnior, STAT3/NF-κB signalling disruption in M2 tumour-associated macrophages is a major target of PLGA nanocarriers/PD-L1 antibody immunomodulatory therapy in breast cancer, Br. J. Pharmacol. 178 (2021) 2284–2304, https://doi.org/10.1111/bph.15373.

[51] M.A.F. Yahaya, M.A.M. Lila, S. Ismail, M. Zainol, N.A.R.N. Afizan, Tumour-associated macrophages (TAMs) in colon cancer and how to reeducate them, J Immunol Res 2019 (2019), 2368249, https://doi.org/10.1155/2019/2368249.

[52] A. Mantovani, T. Schioppa, C. Porta, P. Allavena, A. Sica, Role of tumor-associated macrophages in tumor progression and invasion, Cancer Metastasis Rev. 25 (2006) 315–322, https://doi.org/10.1007/s10555-006-9001-7.

[53] J. Wu, H. Li, H. Xie, X. Wu, P. Lan, The malignant role of exosomes in the communication among colorectal cancer cell, macrophage and microbiome, Carcinogenesis 40 (2019) 601–610, https://doi.org/10.1093/carcin/bgy138.

[54] A. Sica, P. Allavena, A. Mantovani, Cancer related inflammation: the macrophage connection, Cancer Lett. 267 (2008) 204–215, https://doi.org/10.1016/j.canlet.2008.03.028.

[55] O. Warburg, On the origin of cancer cells, Science 123 (1956) 309–314, https://doi.org/10.1126/science.123.3191.309.

[56] I. Manoharan, P.D. Prasad, M. Thangaraju, S. Manicassamy, Lactate-dependent regulation of immune responses by dendritic cells and macrophages, Front. Immunol. 12 (2021), 691134, https://doi.org/10.3389/fimmu.2021.691134.

[57] D. Zhang, Z. Tang, H. Huang, G. Zhou, C. Cui, Y. Weng, C. Liu, S. Kim, S. Lee, M. Perez-Neut, et al., Metabolic regulation of gene expression by histone lactylation, Nature 574 (2019) 575–580, https://doi.org/10.1038/s41586-019-1678-1.

[58] X. Meng, H. Yuan, W. Li, W. Xiao, X. Zhang, Biomarker screening and prognostic significance analysis for renal cell carcinoma, Int. J. Gen. Med. 14 (2021) 5255–5267, https://doi.org/10.2147/IJGM.S325347.

[59] X. Liu, Q. Xu, Z. Li, B. Xiong, Integrated analysis identifies AQP9 correlates with immune infiltration and acts as a prognosticator in multiple cancers, Sci. Rep. 10 (2020), 20795, https://doi.org/10.1038/s41598-020-77657-z.

[60] J. Jing, J. Sun, Y. Wu, N. Zhang, C. Liu, S. Chen, W. Li, C. Hong, B. Xu, M. Chen, AQP9 is a prognostic factor for kidney cancer and a promising indicator for M2 TAM polarization and CD8+ T-cell recruitment, Front. Oncol. 11 (2021), 770565, https://doi.org/10.3389/fonc.2021.770565.

[61] A.S. Verkman, M.O. Anderson, M.C. Papadopoulos, Aquaporins: important but elusive drug targets, Nat. Rev. Drug Discov. 13 (2014) 259–277, https://doi.org/10.1038/nrd4226.

[62] Z. Liu, J. Shen, J.M. Carbrey, R. Mukhopadhyay, P. Agre, B.P. Rosen, Arsenite transport by mammalian aquaglyceroporins AQP7 and AQP9, Proc. Natl. Acad. Sci. U. S. A. 99 (2002) 6053–6058, https://doi.org/10.1073/pnas.092131899.

[63] A.P. Garneau, G.A. Carpentier, A.A. Marcoux, R. Frenette-Cotton, C.F. Simard, W. Rémus-Borel, L. Caron, M. Jacob-Wagner, M. Noël, J.J. Powell, et al., Aquaporins mediate silicon transport in humans, PLoS One 10 (2015), e0136149, https://doi.org/10.1371/journal.pone.0136149.